Scientific Paper

STUDY OF ELECTRONIC STRUCTURE OF TIN-DOPED In_2O_3 (ITO) FILM DEPOSITED ON GLASS

Ali Hassanzadeh, Mohammad Hossein Habibi,* and Asghar Zeini-Isfahani

Department of Chemistry, University of Isfahan, 81745, Isfahan, Iran

Received 31-03-2004

Abstract

Electronic properties of lowly tin doped In_2O_3 (ITO) electrode with nanoscale particles (ca. 36 nm) prepared by electron-beam evaporation on glass substrate in contact with 0.1 mol dm^{-3} H_2SO_4 solution under visible light was investigated by means of linear sweep voltammetry and electrochemical impedance spectroscopy techniques. Differential capacitance results showed that in the high frequency region of EIS data, ITO and impurity element oxides may develops a p-n junction (Esaki tunnel diode) with low charge carrier concentration ($N_D = 2.07\times10^9$ cm^{-3}). In this EIS data region, a reverse semicircle with a negative resistance was appeared. In contrast, in the low frequency region of EIS data, these semiconductors were converted into only n-type one. The flat-band potential of ITO film at low frequency region as determined from capacitance measurements was found to be around -0.0344 volt *vs.* SCE. Also, from the slope of linear portion of Mott-Schottky plot, charge carrier concentration was calculated to be about $N_D = 7.1501\times10^{21}$ cm^{-3}.

Key words: EIS, Mott-Schottky plot, electronic structure, electron beam evaporation, ITO

Introduction

Nanoparticles are generally categorized as the class of materials that fall between the molecular and bulk solid limits, with an average size between 1–50 nm. Nanoparticles exhibit physical and chemical properties different from either the individual molecules or the extended solid.[1,2] Electrochemical and photoelectrochemical properties of nanostructured semiconductor films have attracted considerable interest in recent years due to the quantum-sized effect in comparison with those of the compact polycrystalline or single-crystal ones. Also, the small size of the particles and the presence of semiconductor–electrolyte interface over the whole nanostructured film up to the back contact, reduce the role of a built-in electron field within the particles and increase the importance of the interfacial kinetics.[3] A number of nanocrystalline film electrodes such as TiO_2, ZnO, SnO_2, WO_3, Fe_2O_3, CdSe, CdS (references cited in the ref. 3) and In_2O_3[4] have been studied. It is worth to note that in the case of In_2O_3 nanostructured films only optical and/or electrical properties have mostly been investigated. However, the electrochemical properties of indium oxide and/or ITO in

electrolyte solution are rather poorly known. For instance, Metikos-Hukovic and his co-workers[5] have reported the indium oxide thin film growth as potentiodynamically on the polycrystalline indium substrate and its electrochemical properties have studied in contact with a 0.1 mol dm^{-3} Na-borate buffer (pH=10) solution. Since, the electronic properties (flat band potential and charge carrier concentration) of semiconducting oxides like In_2O_3 depends strongly on different factors such as crystallinity[6] (single or polycrystal), doped material and its amount,[7] the substrate onto which the film was deposited and temperature,[8-10] annealing temperature and atmosphere,[11] and defect density created by external doping or disturbed stoichiometry[12] as well as their growth conditions.[13] Therefore, we can not use the difference of ca. 60 mV/pH unit for flat band potential shift of films which doped with tin (Sn) and prepared by electron beam evaporation technique in solutions with different pH. In order to solve this problem, it is necessary to study the electronic structure of new materials by different techniques. Among the effective techniques for determination of electronic properties, the electrochemical impedance spectroscopy (EIS) is most valuable. To the best of our knowledge according to literatures, less attention has been paid to the study of electronic properties of nanostructured tin doped indium oxide films which have been prepared by electron beam evaporation on glass substrate using EIS technique. Furthermore, it is not clear that the space charge layer capacitance (Mott-Schottky) theory would be apply to these nanocrystalline electrodes in electrochemical cells and quantum efficiency could be obtained from nanocrystalline samples comparable with those of the polycrystalline and single crystal samples. To help answer these questions, we report here capacitance and transmittance data of lowly tin doped In_2O_3 (ITO) electrode with nanoscale particles (ca. 36 nm) which has been deposited using electron-beam evaporation technique on glass substrate.

Experimental

Materials and Apparatus

All materials were of analytical reagent grade and were purchased from Merck and used as received without further purifications. Water used in solution preparation was double distilled. The UV-visible optical transmission spectra were recorded by a double-beam spectrophotometer Cary 500 Scan.

X-ray diffraction study

The phase composition of ITO film deposited on glass was characterized using XRD technique with a D8 Advanced Bruker X-ray diffractometer at room temperature, with monochromated CuKα (λ=1.54 Å) in the scan range of 2θ between 10° to 100° with a step size of 0.03 (2θ/s). Measurements were taken under beam-acceleration conditions of 40 kV/35 mA. The grain size, D, was determined from the FWHM of the strongest line of the XRD peak which correspond to the reflection from the (222) plane at 2θ=30.5° (Figure 1) using the Debye-Scherrer formula.[1]

$$D = \frac{0.9\lambda}{B \times Cos\theta_B} \tag{1}$$

where λ=1.54 Å and B (was 0.239 degree or 3.983×10^{-3} radian in our case) is the measured broadening of the diffraction line peak at an angle of 2θ, at half its maximum intensity (FWHM) in radian and the obtained grain size value for the investigated sample was about 36 nm.

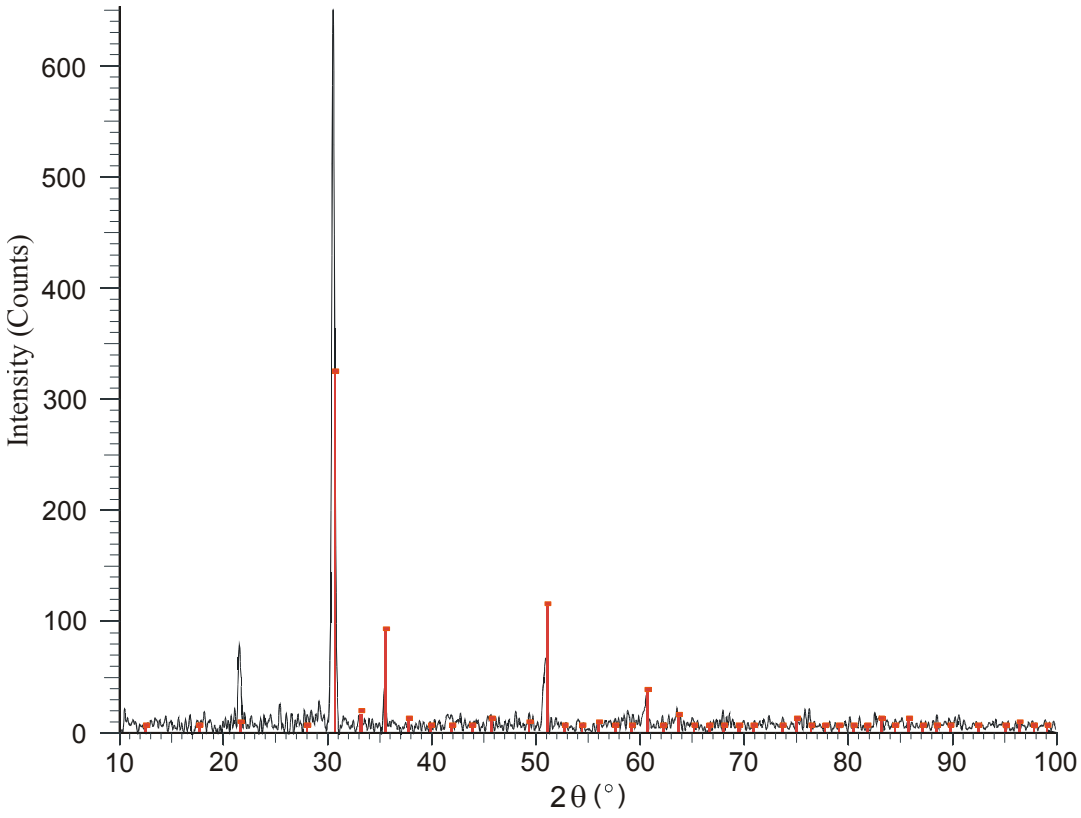

Figure 1. High angle-XRD pattern of lowly tin doped In_2O_3 sample after annealing in air at ca. 500 ºC for 24 h. The bar graphs represents XRD pattern of In_2O_3 sample.

Electrochemical measurements

The electrochemical measurements were performed in a conventional three-electrode cell under visible light. The solution volume was ca. 50 ml. A lowly tin doped In_2O_3 (ITO) film electrode on glass substrate with nanoscale particles which has been made by electron-beam evaporation was used as working electrode. The target material used to make the working electrode was an ITO pellet which has been analyzed with XRF technique with composition in wt. %: In_2O_3, 89.75; SnO_2, 9.42; CaO, 0.12; K_2O, 0.096; Fe_2O_3, 0.069; CuO, 0.069; UO_2, 0.026; ZnO, 0.025 and Al_2O_3, 0.025. The thickness of film was determined by quartz crystal microbalance measurements and the obtained value for the investigated sample was about 45 nm. After deposition, electrode was annealed in air at ca. 500 °C for 24 h to ensure good electrical contact between particles and then quenched in air at the room temperature. The geometric surface area of working electrode exposed to solution was 9.6 cm^2 (1.90 cm×5.05 cm). A cylindrical vessel was used as electrochemical cell in which the whole size of working electrode was immersed in the solution. The counter electrode was a large-area platinum gauze, which is particularly important for impedance measurements (impedance of a counter electrode must be negligible in comparison with a working electrode) and an $Hg|Hg_2Cl_2$, (saturated KCl) (SCE) as the reference electrode. Linear sweep voltammetry and cyclic voltammetry are performed using Autolab GPES (Eco Chimi B.V.) with a scan rate of 100 mV s^{-1} and electrochemical impedance spectra were measured with Autolab FRA module (Eco Chimi B.V.) by applying sinusoidal voltage with amplitude of ±10 mV and frequency ranges from 100 kHz to 0.1 Hz. All EIS spectra were fitted to the electrical equivalent circuits using Zveiw program developed by J. R. Mcdonald.[14]

Results and discussion

Linear sweep voltammetry

The results of linear sweep voltammetry and cyclic voltammetry experiments of lowly tin doped In_2O_3 film with a scan rate of 100 mV/s in 0.1 mol dm^{-3} H_2SO_4 (pH=0.98) solution are shown in Figure 2A,B. Although, the overvoltage of hydrogen and oxygen evolution on the In_2O_3 surface is relatively high (i.e. ca. 1 and 0.5 volt) and corresponding peaks appear at ca. -0.8 and +1.5 volt *vs.* SCE in pH=0.98, respectively,[5] to prevent side reactions and evolution of H_2 and/or O_2 gasses, the range of applied

potential was from -0.5 to 1 volt *vs.* SCE. During anodic polarization, a cathodic current is showed over potential range between -0.5 and -0.2 volt *vs.* SCE. This cathodic current is probably related to the reduction of In_2O_3 or with evolution of hydrogen. It can also be seen that there is an anodic peak around -0.2 volts *vs.* SCE. Since, the processes of the indium oxide formation is characterized by a well defined peak[5] at a potential around -0.5 volt *vs.* SCE in pH=0.98 and the formation of Sn(II)-oxide/hydroxide and the formation of Sn(IV)-oxide/hydroxide layers take place at potential -0.494 and -0.394 volt vs. SCE, respectively in pH=0.98,[15] the assignment of this anodic peak is very difficult. It seemed that the impurities may cause to develop a p-n junction that controls their electronic structure. According to the physics of semiconductors,[16] this feature can be related to the formation of a tunnel (Esaki) diode as an n-type and a p-type junction which can easily be detected by Mott-Schottky plot of high frequency EIS data (will be discussed later). A tunnel diode is a semiconductor device with a negative resistance which is made very much like an ordinary alloyed p-n rectifier, except that both p- and n-regions as heavily doped as possible; a typical tunnel diode may have doping densities of 10^{18} or 10^{19} carrier per cm^3 in both p- and n-regions.[17] It operation depends upon a quantum mechanic principle known as "tunneling" wherein the intrinsic voltage barrier is reduced due to doping levels which enhance tunneling. The negative resistance region is the important characteristic for the tunnel diode and did not appear in I-E plot of conventional diodes. In this region, with increasing voltage the current decreased just the opposite of a conventional diode. The most important specifications for the tunnel diode are the peak voltage (E_p), peak current (I_p), valley voltage (E_v), and valley current (I_v) (Figure 2). The anodic current region of Figure 2 was scale-expanded as an inset to represent these features. Clearly, in the potential region more positive than the -0.2 volt to 0.2 a negative polarization resistance appeared which is the characteristic of tunnel diodes and decaying current is due to band-to-band tunneling effect. Then, the current is limited to a very low level and this potential region is called "valley". For a voltage larger than valley potential (ca. 1 volt *vs.* SCE in our case) the current increases exponentially with voltage (not shown here). The observed anodic current from point *b* to *d* is a summation of tunnel current, excess current due to trapping impurities or structural imperfections and majority carrier diffusion current.[17]

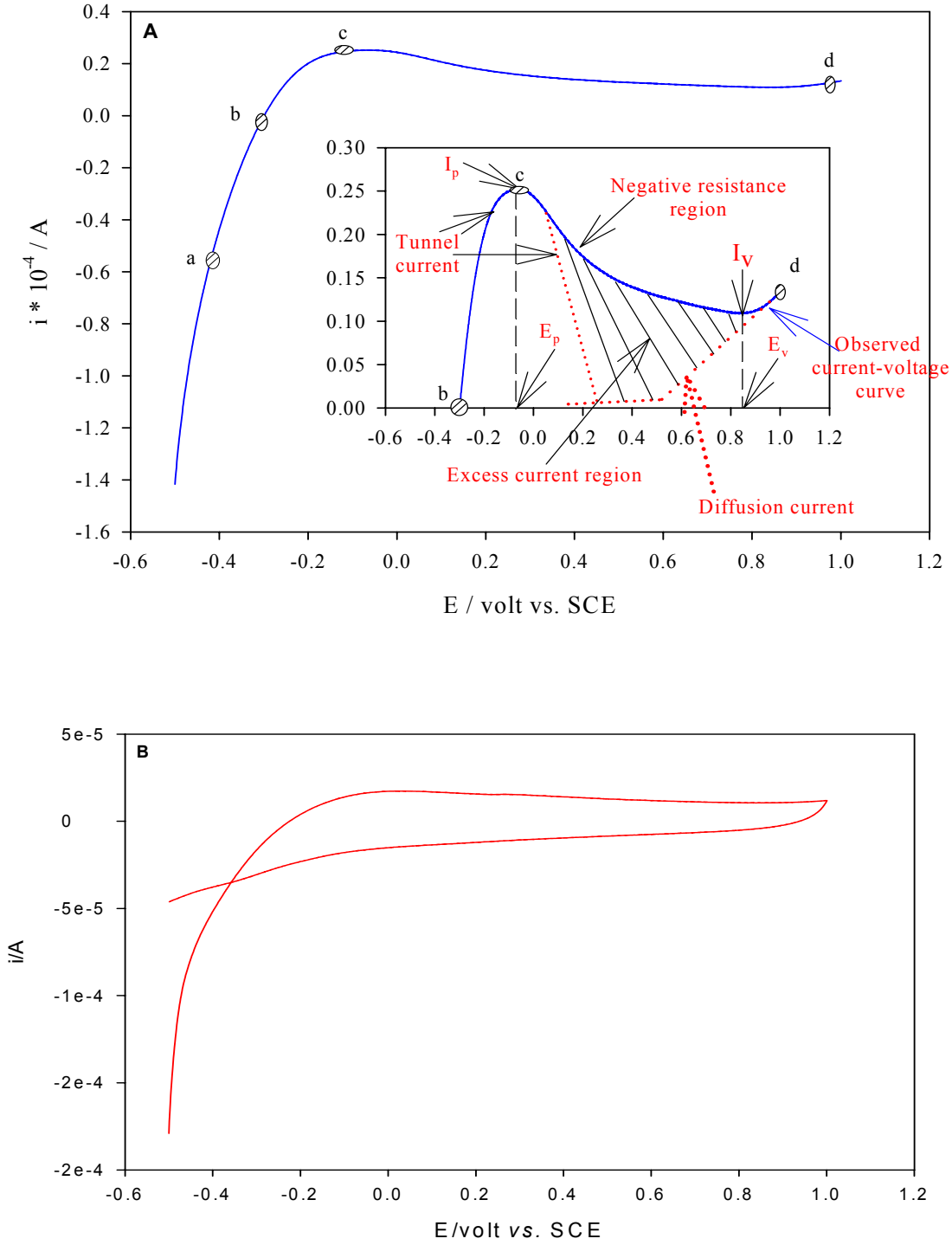

Figure 2. A) Linear sweep and B) Cyclic voltammetry curves of lowly tin doped In_2O_3 film electrode with a scan rate of 100 mV/s in contact with 0.1 mol dm^{-3} H_2SO_4 solution. The inset is the detail of tunnel diode currents contributions.

Impedance Studies

The complex plane plots and Bode plots of lowly tin doped In_2O_3 film electrode in contact with 0.1 mol dm^{-3} H_2SO_4 solution were shown in Figures 3 and 4. The high-frequency EIS response of complex plane plots was scale-expanded, as presented in the inset of Figure 3. Each of these impedance spectrum in complex plane plots can be divided into three distinct frequency regions; (i) In the high frequency region (between 100 kHz and ca. 4 kHz), a time constant as a dispersed reveres semicircle indicating a negative polarization resistance has been emerged which has little significant variation with electrode potential changes. It is well known that the negative resistance is a direct consequence of the negative slope in the current/voltage curve just above the passivation voltage and is mostly observed in the corroding cases. Besides, it is also well documented that the most common source of negative resistance in electrochemical systems results from an interplay between adsorption and electrodissolution, giving rise to a current that decreases with increasing voltage for $\omega \to \infty$, even though the interfacial differential capacitance is positive.[18] One of the other case where this feature could be seen is an Esaki or tunnel diode. We attributed this feature to the development of a tunnel diode and band-to-band majority carrier tunneling.

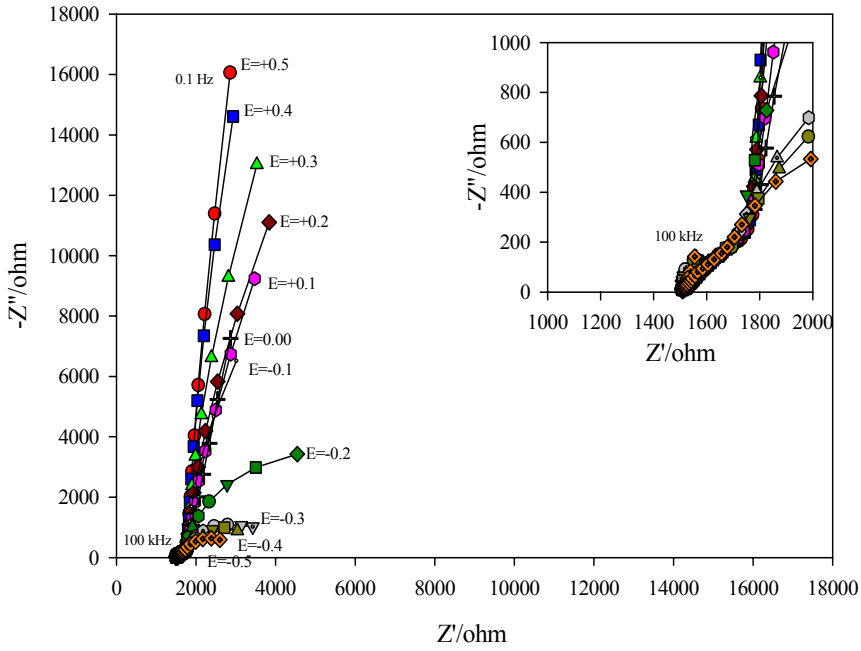

Figure 3. Complex plane plots of lowly tin doped In_2O_3 film electrode in contact with 0.1 mol dm^{-3} H_2SO_4 solution under visible light at different potentials from -0.5 to 0.5 volt *vs.* SCE. The inset is high-frequency EIS response with scale-expanded.

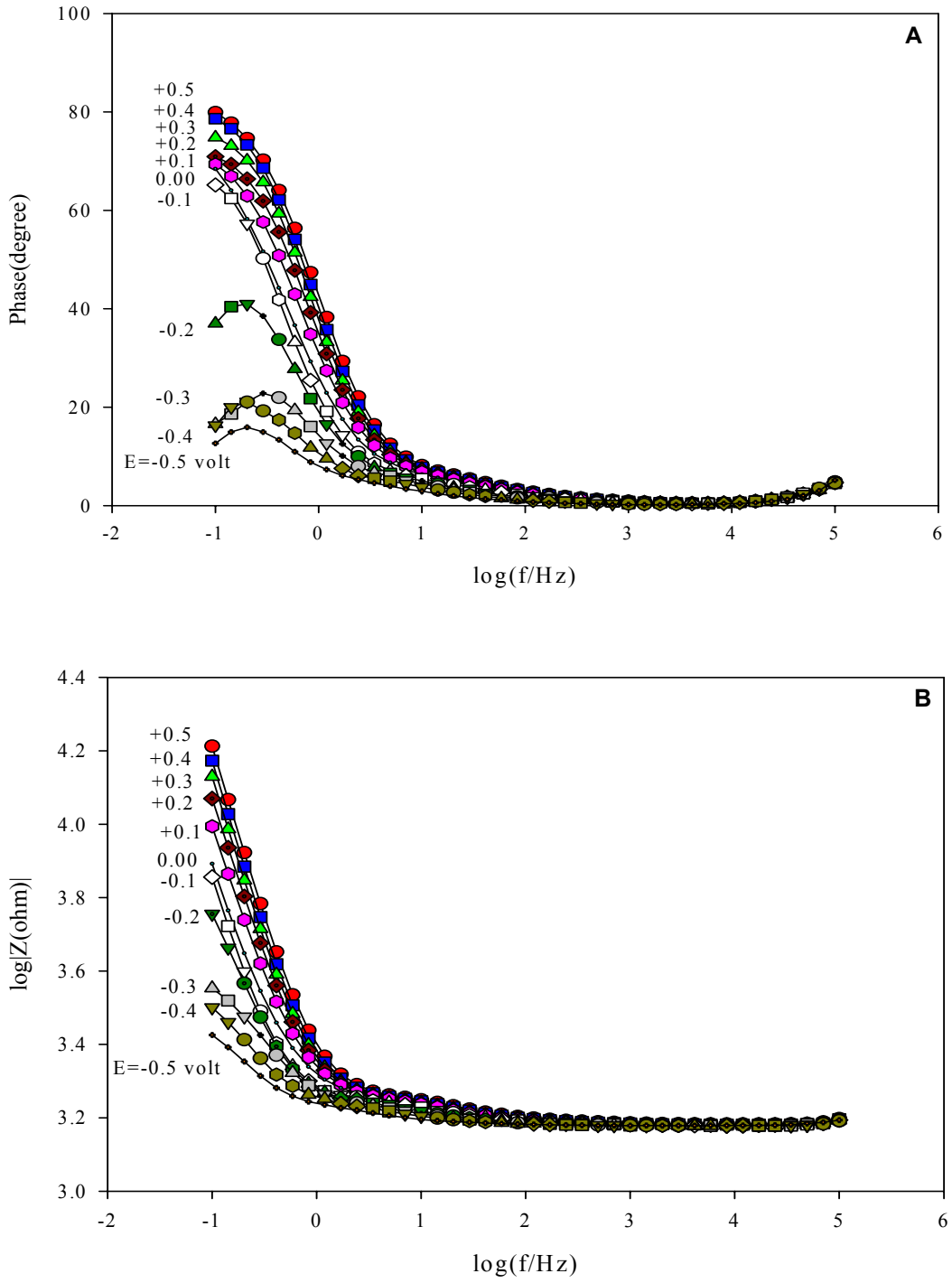

Figure 4. Bode: A) phase and B) magnitude plots of lowly tin doped In_2O_3 film electrode in contact with 0.1 mol dm^{-3} H_2SO_4 solution under visible light at different potentials from -0.5 to 0.5 volt *vs.* SCE.

(ii) The medium frequency range of impedance spectra (between 4 kHz and ca. 20 Hz), corresponds to a straight line with an angle of about 45° in the whole spectra. This linear dependence of the imaginary and real part of impedance is related to the diffusion

processes, which called "Warburg impedance". But, the fitting procedure showed better agreement between theoretical and experimental data if a frequency dependent constant phase element (CPE) in parallel with a resistance is introduced instead of Warburg impedance. Generally, the appearance of a CPE is due to a distribution of the relaxation times as a result of inhomogenities presented at the microscopic level of the oxide phase and at the oxide | electrolyte interface contributions from static disorder such as porosity, a random mixture of conductor and insulator that can be described by the effective medium approximation as percolation or an interface that can be described by fractal geometry or a RC transmission line.[5] The impedance of a constant phase element is defined as:

$$Z_{CPE} = [T(j\omega)^p]^{-1} \qquad with \qquad -1 \le p \le 1 \tag{2}$$

where Z_{CPE} is the electrode impedance, the constant T is a combination of properties related to both the surface and the electroactive species and is independent of frequency, the exponent p is related to a slope of the logarithm of Z_{CPE} against logarithm of frequency Bode plot, and $j=(-1)^{0.5}$. A pure capacitance yields p=1, a pure resistance yields p=0, while p=0.5 represents Warburg impedance. For our lowly tin doped In_2O_3 film electrode the fitting yielded p values are very close to 0.5 which might suggest a diffusion process and can be explained by diffusion of majority carriers from conduction band of a n-type and/or from valance band of a p-type semiconductor towards depletion layer at p-n interface[16,17] and accumulating in there. Since, the tunneling process is practically instantaneous in comparison with diffusion phenomena,[17] therefore the tunneling will appear in high frequencies in EIS spectra. Hence, this diffusion feature can not be related to the tunneling effect. The Randles plot was used to further confirmation of diffusion phenomenon. (iii) In the low frequency region (between ca. 20 Hz and 0.1 Hz), the spectra change with potential in manner which is characteristic of a space charge layer. The diffusion of majority carriers towards depletion layer and its accumulation in there might cause this phenomenon. In order to support this statement, we need to calculate charge carrier concentration in the depletion layer at high and low frequency regions which in turn needs Mott-Schottky plot.[19]

Randles plot analysis

The impedance responses of ITO film in frequency region between 4 kHz and ca. 20 Hz at bias potential of 0.5 volt *vs.* SCE represented as a Randles plot[20] in Figure 5. The Randles plot is useful in determining whether Warburg impedance is a significant component of the equivalent circuit model. A plot of both, the real and imaginary parts of Z *vs.* $\omega^{-1/2}$ should give straight lines with equivalent slopes and these traces will not be parallel for features other than the Warburg impedance. Thus, the linearity of Randles plot can be used as a test of diffusion control and Warburg diffusion coefficient (σ) can also be calculated from each of these slopes. If the obtained lines are not parallel then the theory cannot be applied (i.e. the feature is not related to diffusion control processes but will be due to another process), or the experimental accuracy is not good. As shown in Figure 5, the obtained lines are parallel; therefore this behavior without any doubt is due to diffusion control phenomenon. A similar trend was observed for other bias potentials which were not shown here. The values of their slopes are presented in Table 1.

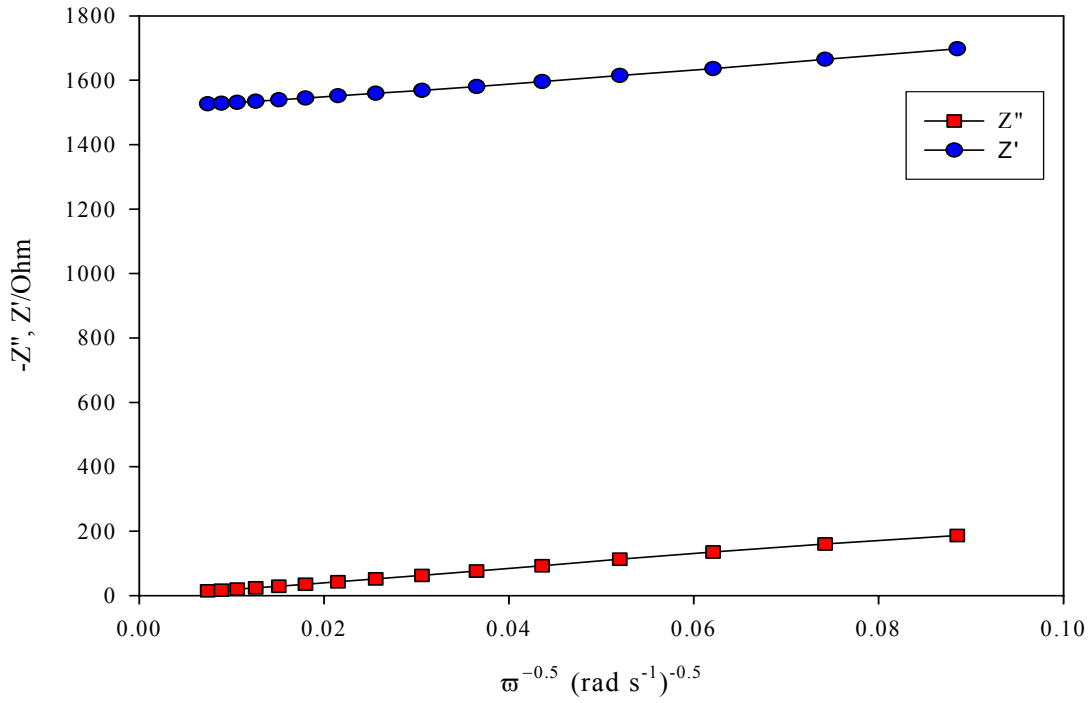

Figure 5. Randles plot of lowly tin doped In_2O_3 film electrode in contact with 0.1 mol dm^{-3} H_2SO_4 solution via 0.5 volt bias potential vs. SCE.

Equivalent circuit selection

The selection of electrical equivalent circuits was used on the following facts; i) Previous results obtained using linear polarization technique which indicates negative resistance and a reverse semicircle capacitive behavior in high frequency region in the complex plane plot, ii) Randles plot which indicates Warburg impedance element, iii) Charge carrier accumulation behavior (capacitive behavior) in low frequency regions of EIS data and with considering the electrical equivalent circuit in Ref. 16 (page 532). We have used two types of electrical equivalent circuits to resolve the complex processes within Nyquist plots of ITO film electrode in contact with 0.1 mol dm^{-3} H_2SO_4 solution at bias potential range between -0.5 and 0.5 volt *vs.* SCE. The dispersion in the spectra of 0.5 to -0.1 volt *vs.* SCE could be interpreted by equivalent circuit shown in Figure 6a and other spectra of -0.2 to -0.5 volt *vs.* SCE could be interpreted by equivalent circuit shown in Figure 6b. Our attempts to approximate low frequency part in Figure 6b with a parallel RC circuit failed, and a reasonable fit was only obtained when C replaced by a constant phase element (CPE4). It is also worth to note that the resistance R4 in Figure 6b in some cases was omitted in order to obtain better fitting parameters. The parameters of the complex non-linear least square fitting using Zview program are presented in Table 2.

Table1. Randles plots parameters of lowly tin doped In_2O_3 film electrode at different applied bias potentials using linear least square fitting with straight line equation for individual experimental impedance data.

Potential (volt vs. SCE)	*-Z″ (slope)* Ohm $(rad\ s^{-1})^{1/2}$	*-Z″* (R^2)	*Z′ (slope)* Ohm $(rad\ s^{-1})^{1/2}$	*Z′ (intercept)* Ohm	*Z′* (R^2)
+0.5	2126.5	0.9982	2101.6	1507.3	0.9978
+0.4	2017.5	0.9982	1989.1	1503.1	0.9972
+0.3	1894.9	0.9960	1864.3	1499.9	0.9934
+0.2	1854.9	0.9970	1797.6	1499.0	0.9966
+0.1	1752.3	0.9979	1713.5	1498.8	0.9969
0.00	1633.8	0.9988	1624.5	1500.0	0.9973
-0.1	1416.8	0.9991	1450.6	1498.7	0.9991
-0.2	1150.4	0.9992	1125.6	1498.7	0.9993
-0.3	983.7	0.9955	901.77	1499.1	0.9963
-0.4	799.35	0.9937	693.2	1501.2	0.9945
-0.5	583.23	0.9884	476.51	1504.0	0.9877

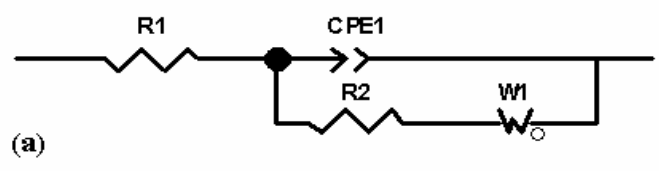

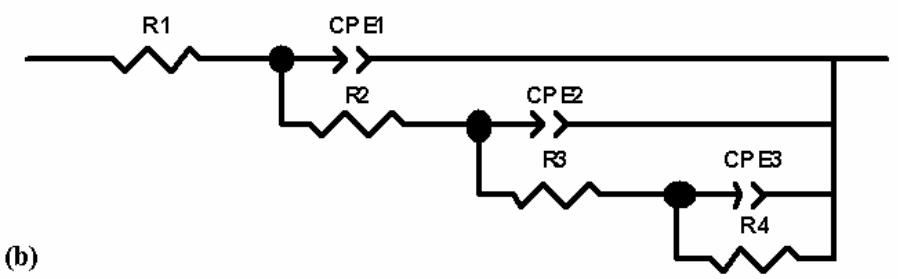

Figure 6a and 6b. Electrical equivalent circuits for lowly tin doped In_2O_3 film electrode in which R1 to R4 are resistances, CPE1 to CPE3 are constant phase elements and Wo (W1) is finite length diffusion element.

Table 2. Equivalent circuit parameters of lowly tin doped In_2O_3 film electrode in contact with 0.1 mol dm^{-3} H_2SO_4 solution over potential range between -0.5 and 0.5 volt *vs.* SCE based on Figures 6a and 6b.

Potential* / Element	+0.5	+0.4	+0.3	+0.2	+0.1	0.00	-0.1	-0.2	-0.3	-0.4	-0.5
R1(Ω)	2268	2194	2394	2561	2363	2831	2280	1778	1914	1862	11211
CPE1-T ($\Omega^{-1}s^p$)	3.67 e^{-11}	5.72 e^{-11}	2.25 e^{-11}	1.33 e^{-11}	1.88 e^{-11}	7.37 e^{-12}	5.43 e^{-11}	2.10 e^{-8}	1.81 e^{-9}	3.79 e^{-9}	1.71 e^{-13}
CPE1-P	1.181	1.161	1.19	1.20	1.21	1.22	1.14	0.85	0.97	0.93	1.19
R2(Ω)	-763.5	-694.3	-898.5	-1069	-872.3	-1339	-783.2	-263.3	-406.2	-351.2	-9701
W_O-*R(Ω)*	799.6	780.6	716.1	665.4	686.2	762.0	656.1	–	–	–	–
W_O-*T(s)*	0.072	0.077	0.074	0.074	0.089	0.130	0.133	–	–	–	–
W_O-*P*	0.484	0.483	0.472	0.459	0.452	0.451	0.460	–	–	–	–
CPE2-T ($\Omega^{-1}s^p$)	–	–	–	–	–	–	–	1.12 e^{-4}	2.3 e^{-4}	2.23 e^{-4}	3.81 e^{-4}
CPE2-P	–	–	–	–	–	–	–	0.81	0.71	0.77	0.75
R3(Ω)	–	–	–	–	–	–	–	413.2	534.1	395.4	426.8
CPE3-T ($\Omega^{-1}s^p$)	–	–	–	–	–	–	–	1.66 e^{-4}	1.58 e^{-4}	3.43 e^{-4}	4.52 e^{-4}
CPE3-P	–	–	–	–	–	–	–	1.02	1.09	1.00	1.08
R4(Ω)	–	–	–	–	–	–	–	7768	2378	1996	1193

* Potential vs. SCE.

The diffusion coefficient of main charge carriers was calculated from the results of Table 2 and Equation 3[14]

$$T = L^2 / D \tag{3}$$

where D is diffusion coefficient of charge carriers, L is effective diffusion length and T is finite length diffusion element exponent (i.e. Wo-T). By substituting L=45 nm in Equation 3 which is a reasonable value for thin films,[21] and Wo-T values from Table 2, the diffusion coefficient of charge carriers as a function of bias potential were obtained (Table 3). The obtained values are of the order of 10^{-10} cm^2 s^{-1}, for the potential region considered. Such a low value of diffusion coefficient clearly indicates that the diffusion processes occur in the solid phase.

Table 3. Diffusion coefficient of main charge carriers of ITO thin film in contact with 0.1 mol dm^{-3} H_2SO_4 solution over potential range between -0.1 and 0.5 volt *vs.* SCE.

Potential (Volt) vs. SCE	W_o-T (s)	Diffusion coefficient $\times 10^{-10}$ (cm^2 s^{-1})
+0.5	0.072	2.812
+0.4	0.077	2.629
+0.3	0.074	2.736
+0.2	0.074	2.736
+0.1	0.089	2.275
0.00	0.130	1.557
-0.1	0.133	1.522

Mott-Schottky plot analysis

The Mott-Schottky theory[20,21] is commonly used to evaluate electronic properties of semiconductors by using the following equations:

$$\frac{1}{C_{sc}^{\ 2}} = \left(\frac{2}{e\varepsilon\varepsilon_0 A^2 N_D}\right)\left(E - E_{FB} - \frac{\kappa T}{e}\right) \quad \text{For n-type semiconductor} \tag{4}$$

$$\frac{1}{C_{sc}^{\ 2}} = \left(\frac{2}{e\varepsilon\varepsilon_0 A^2 N_A}\right)\left(-E + E_{FB} - \frac{\kappa T}{e}\right) \quad \text{For p-type semiconductor} \tag{5}$$

where ε_0 is the permittivity of free space, ε, the static dielectric of the semiconductor, e, the electron charge, κ, the Boltzmann constant, T, absolute temperature, N_D and N_A, the donor and acceptor concentration, $C_{sc,}$ the space charge layer capacitance, E_{FB}, flat band potential, A, real surface area of electrode and E, the electrode bias potential. In the absence of deep-level electronic states, a plot of the inverse square of the capacity of

space charge layer as a function of applied bias potential give a linear line with a voltage intercept equal to the flat band potential and a slope of inversely proportional to the donor concentration. The differential capacitance values of a lowly tin doped In_2O_3 film electrode were obtained by means of impedance spectroscopy measurements at fixed potential. For high frequency regions the CPE1 exponents (CPE1-P) were found to be in the range 1.14 to 1.22. Due to its relatively insignificant deviation of the CPE1 exponents from unity (and its weak dependence on potential), the pre-exponential coefficient of the CPE element (CPE1-T) was considered as a reciprocal capacitance. Then, the electrode differential capacitance *vs.* applied bias potential was shown in the form of the Mott-Schottky plot in Figures 7a and 7b for high and low frequency regions in 0.1 mol dm^{-3} H_2SO_4 solution over potential range between -0.5 and 0.5 volt *vs.* SCE, respectively. In the Mott-Schottky diagram which was plotted at high frequency, two different semiconductors as an n-type and a p-type were developed which each of these have different flat-band potentials. The values of ca. -0.1 and ca. 0.4 volt *vs.* SCE were obtained from extrapolation of individual lines. By substituting high frequency dielectric constant of 3.4 for the tin doped In_2O_3 film[22] in Equation 4, charge carrier concentration was obtained only for n-type, $N_D = 2.07\times10^9$ cm^{-3}.

P-type semiconductivity has been observed for some d-metal chalcogenides and halides with lower oxidation numbers, including Cu_2O, FeO, FeS, and CuI. Several d-metal oxides, including ZnO and Fe_2O_3, are n-type semiconductors.[23] Since, XRF analysis was done before annealing and we did not analyzed of the sample after annealing, therefore, we can not answer what the origin of p-type semiconductivity is and unable to calculate acceptor concentration at high frequency. On the other hand, in the Mott-Schottky diagram plotted at low frequency, the In_2O_3 film showed only n-type semiconductor behavior. A linear relationship between the squared reciprocal of capacitance and potential was observed in the range of 0.0 to 0.5 volt *vs.* SCE. By extrapolate of this part and its intersection with the potential axis, the flat-band potential was determined (-0.0344 volt *vs.* SCE). The charge carrier concentration was determined from the slope of liner part using Equation 4 by inserting 3.4 for the value of dielectric constant and considering the value of electrode roughness factor to be 1 and neglecting the Helmholtz layer capacitance ($N_D = 7.1501\times10^{21}$ cm^{-3}). This value of N_D is in a good agreement with published values.[24,25] The strong frequency dependence of capacitance curves at high and low frequencies can be interpreted by the fact that, at low

frequency, the lattice oxygen could be removed to the solution according to the Equation 6.[5] While at high frequency this dose not occur. Therefore, in the low frequency region in addition to electron-hole transfer, oxygen vacancies have a significant influence in the electrode capacitance, while in high frequency region only electron-hole translation is dominant.[18]

$$In_2O_{3(s)} + 6H^+ + 6e^- \rightarrow 2\ In_{(m)} + 3\ H_2O_{(aq)} \quad (6)$$

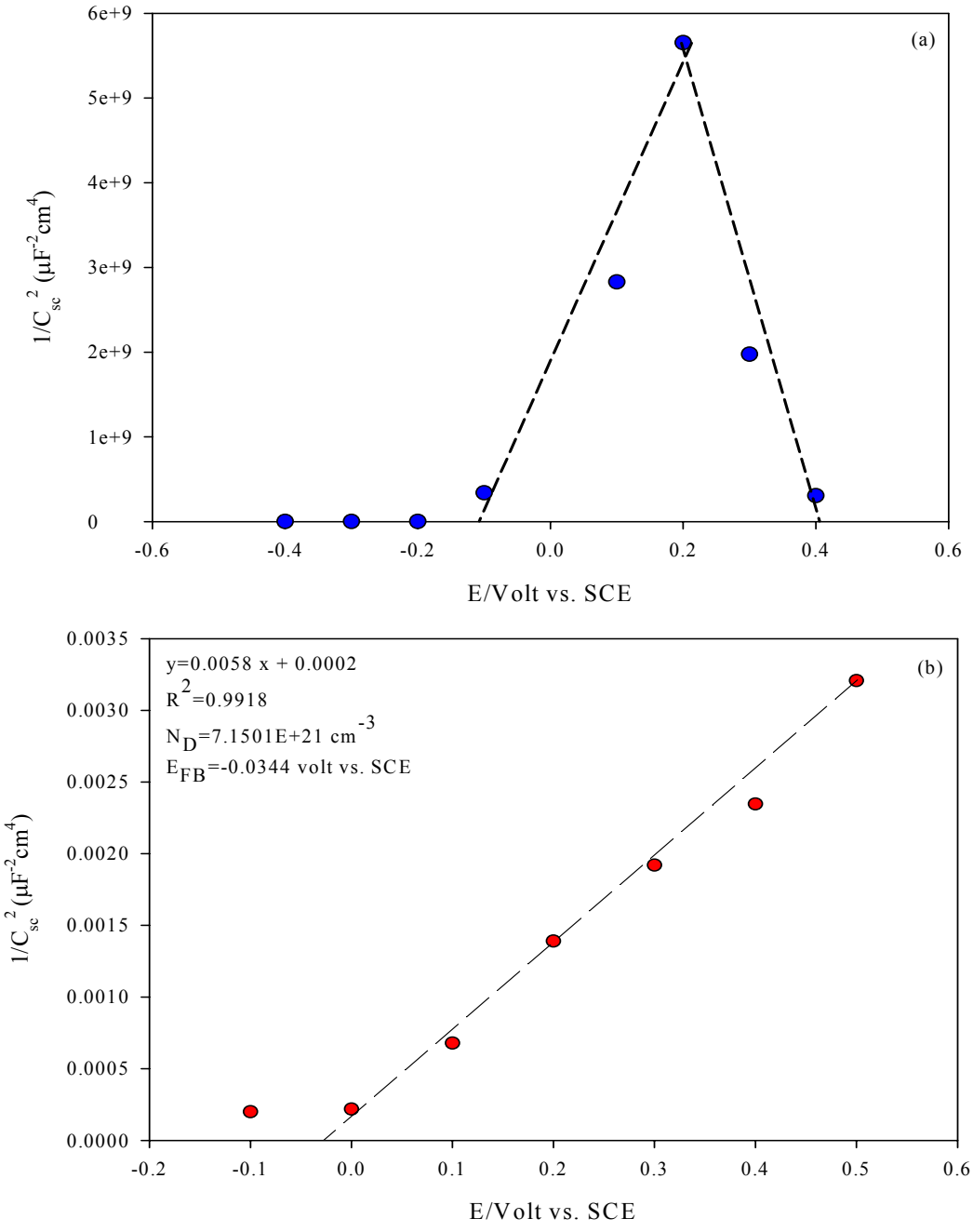

Figure 7. (a) High and (b) low frequency region Mott-Schottky plots of lowly tin doped In_2O_3 film electrode in 0.1 mol dm^{-3} H_2SO_4 over potential range between -0.5 and 0.5 volt *vs.* SCE.

Quantum efficiency

In order to compare quantum efficiency of nanocrystalline lowly tin doped In_2O_3 film electrode with poly and/or single crystal samples, it is necessary to calculate the width of space charge layer (Wsc). This width is determined by Equation 7.[26] The calculated values of space charge width as a function of polarization potential is presented in Figure 8. By increasing bias potential, the width of space charge layer was also increased.

$$W_{sc} = [\frac{2 \times \varepsilon\varepsilon_0}{e \times N_D}(E - E_{FB})]^{\frac{1}{2}} \quad (7)$$

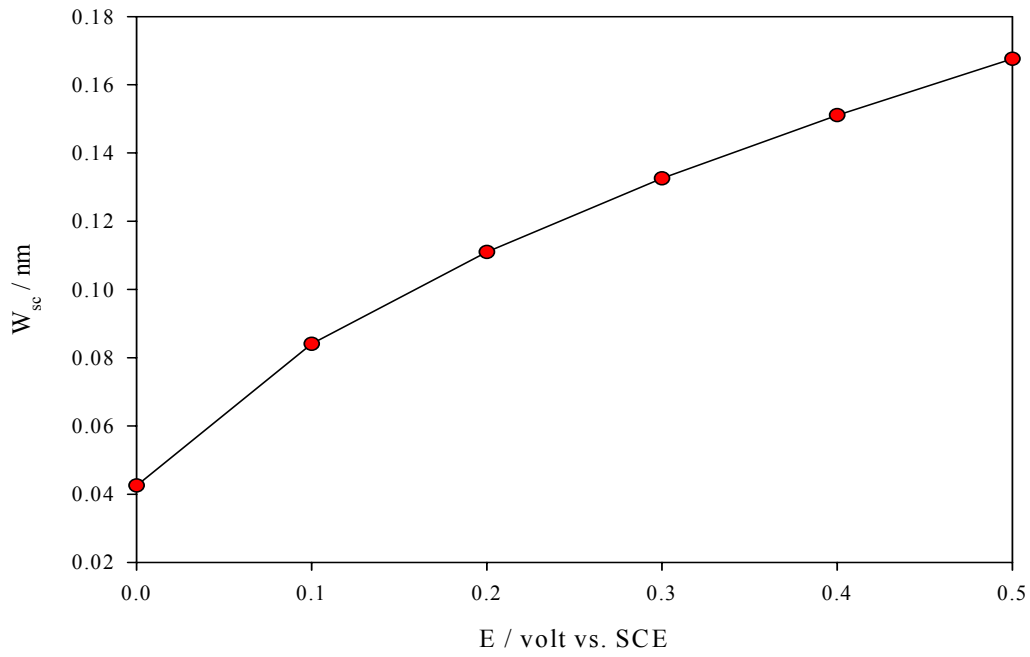

Figure 8. Dependence of space charge layer width (W_{sc}) on the applied bias potential for a lowly tin doped In_2O_3 film electrode in 0.1 mol dm^{-3} H_2SO_4 over potential range of 0.00 and 0.50 volt *vs.* SCE.

The quantum efficiency, Q, defined as the number of charge carriers measured in the external circuit for each photon absorbed, is determined by the flux of minority carriers arriving at the surface j_p and by losses due to surface recombination of electrons and holes. For the case in which surface recombination can be disregarded the Gärtner model[27] describes the dependence of the quantum efficiency on depletion layer width (Wsc) and absorption coefficient of the light ($\alpha(\lambda)$) by Equation 8.

$$Q = \frac{j_p}{\phi} = 1 - \frac{e^{-\alpha(\lambda)\times W_{sc}}}{1 + \alpha(\lambda) \times L_p} \tag{8}$$

From this equation it is clear that in order to ensure a significant quantum efficiency it is necessary that L(λ) < Wsc or L(λ) < Lp. The penetration depth of the light L(λ) is usually defined as L(λ)=1/α(λ). Where Lp is the minority carrier diffusion length and α(λ) is absorption coefficient of the light.[21]

Figure 9A-C shows the dependence of transmittance percent on the wavelength, dependence of absorption coefficient of the light on the wavelength, and plot of $(\alpha h\upsilon)^{1/2}$ vs. $h\upsilon$ (allowed indirect transitions) for lowly tin doped In_2O_3 thin film which absorption coefficient α(λ) values can be obtained from transmission, T, data using Equation 9 where d (=45 nm) is the thickness of the ITO film.

$$\alpha(\lambda) = \frac{\ln(1/T)}{d} \tag{9}$$

The calculated allowed indirect band gap for our case by using Figure 9C is ca. 3.80 eV, corresponding to a wavelength of 326.31 nm. For λ=300 nm, $\alpha(\lambda)$ is 0.04 nm^{-1} giving

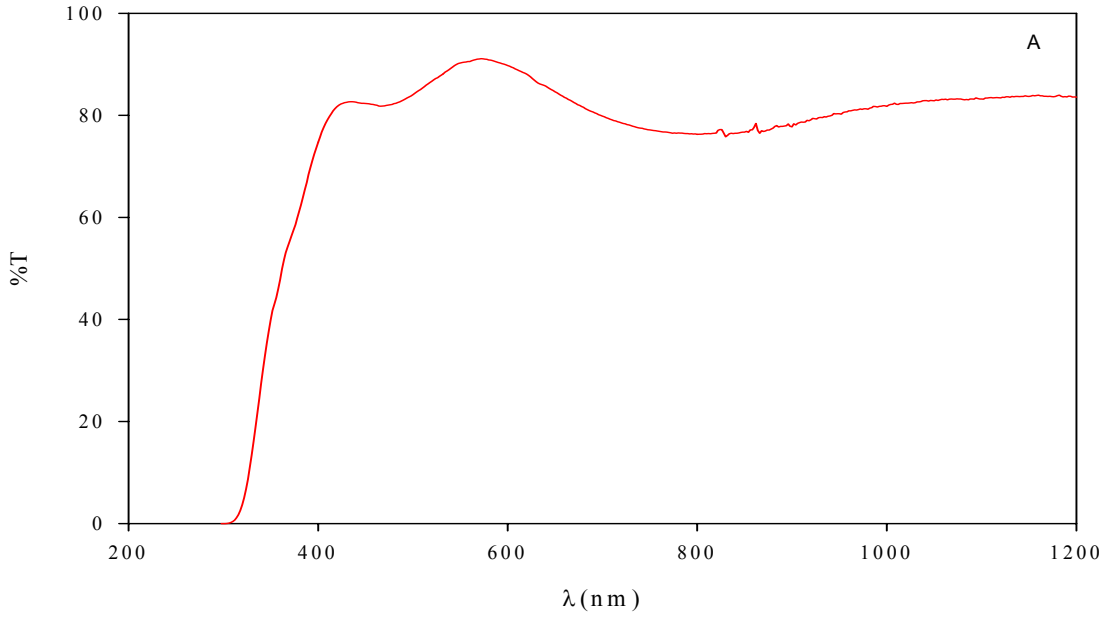

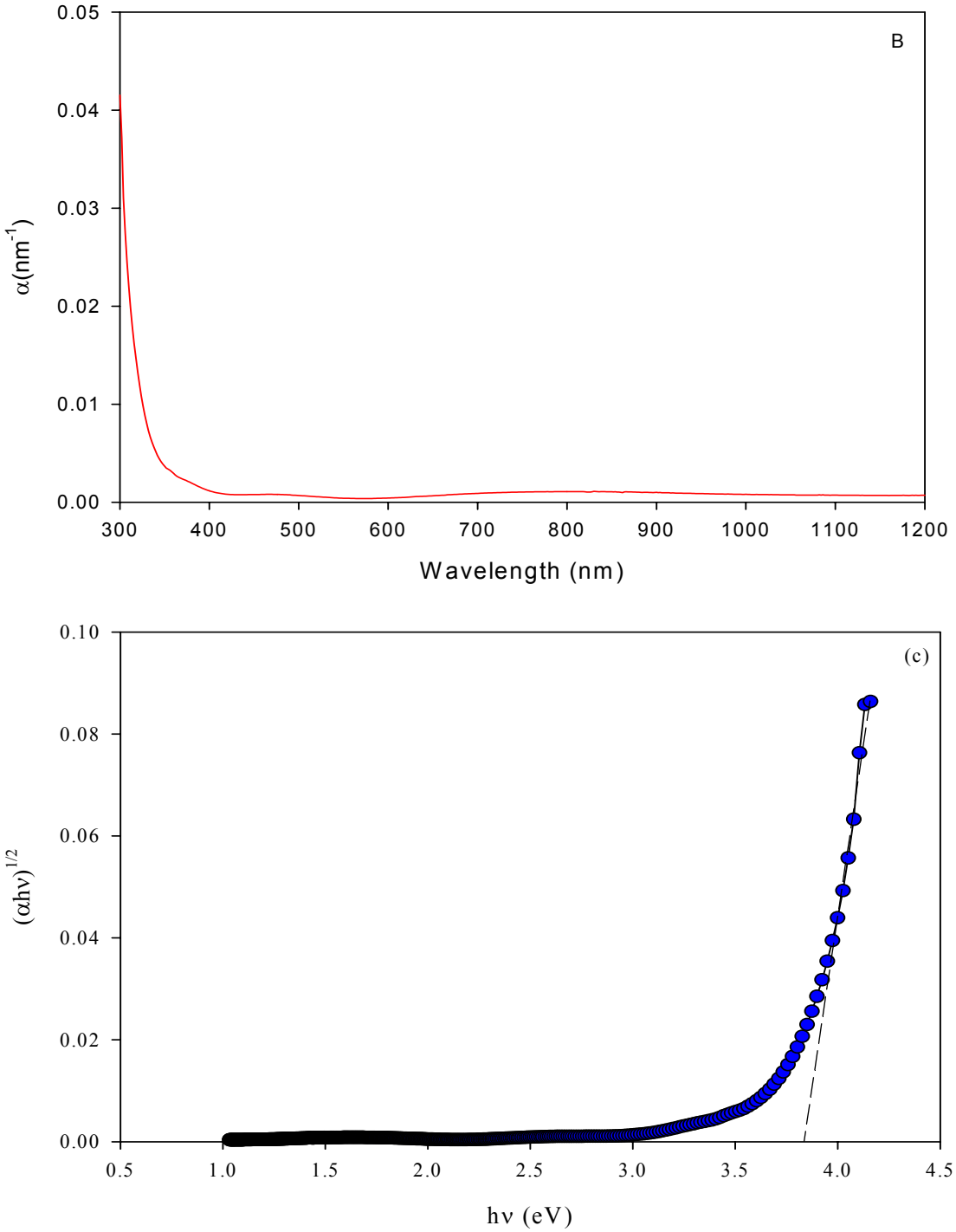

Figure 9. A) Dependence of transmittance percent on the wavelength, B) Dependence of absorption coefficient of the light on the wavelength, and C) Plot of $(\alpha h\upsilon)^{1/2}$ *vs.* $h\upsilon$ (allowed indirect transitions) for lowly tin doped In_2O_3 thin film.

the penetration depth of the light L(λ)=25 nm and considering the minority carrier diffusion length L_p=25 nm and W_{sc}=0.167 nm. With substitution of these quantities into Equation 8, a quantum efficiency of about 50% is found for this ITO film, while, the

band gap of GaP is 2.24 eV, corresponding to a wavelength of 554 nm. For λ=514 nm, $\alpha(\lambda)$ is 10 cm^{-1} giving L(λ)=10 μm, a typical value for L_p in n-type GaP is 50 nm. The depletion layer width at a band bending of 1 eV is of the order of 50 nm for a moderate doping level. A quantum efficiency of only about 1% is found in this case which shows that the most of the electron/hole pairs recombine in the bulk of the semiconductor.[21] Figure 10 shows the dependence of quantum efficiency percent of lowly tin doped In_2O_3 thin film against the wavelength of light.

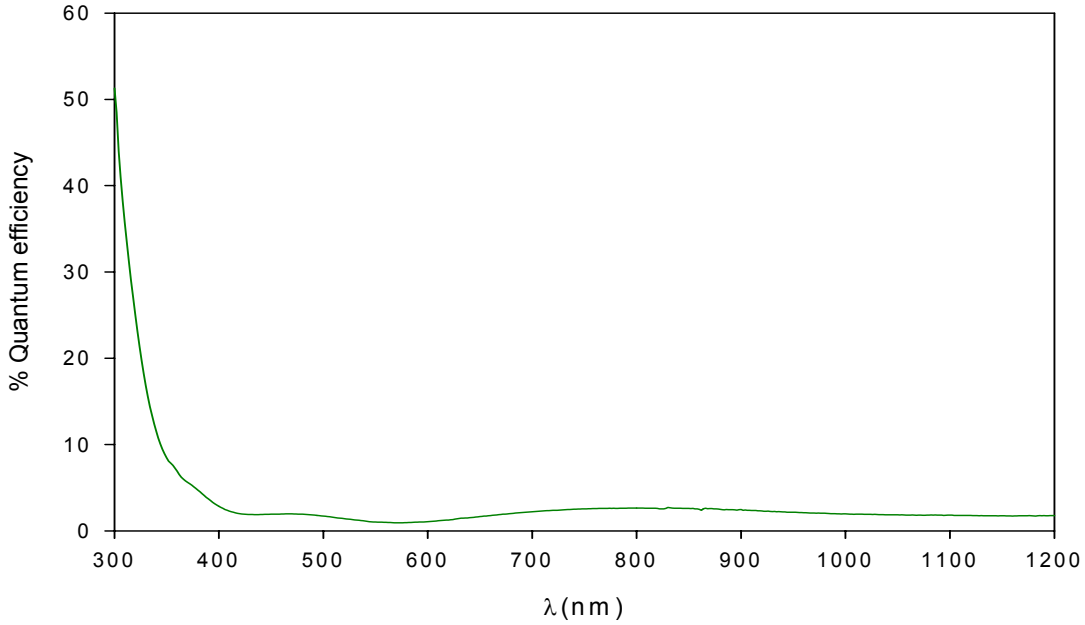

Figure 10. Dependence of quantum efficiency percent of lowly tin doped In_2O_3 thin film on the wavelength of light based on the Gärtner model with considering L_p=25 nm and W_{sc}=0.167 nm.

Conclusions

The following conclusions could be drawn from the present study:

1. Electrochemical impedance spectroscopy can be used to a successful model of a nonostructured lowly tin doped In_2O_3 film semiconductor–electrolyte interface.
2. The lowly doping of tin into the In_2O_3 lattice formed a highly degenerate n-type semiconductor which has strong frequency dependence capacitance in acidic solution and the etching of thin films in acidic solution causes increasing of the film conductivity. This behavior is related to electron-hole and oxygen vacancy contributions in electrode capacitance and conductance.
3. The electronic characteristics of the ITO semiconductor film (i.e. flat band potential and charge carrier concentration in the space charge layer) were strongly dependent on the deposition and annealing conditions, particularly to heat

treatment environment (oxygen concentration) and the impurities of target material. Furthermore, the solubility of ITO thin film in solution has significant effect as well.

4. Electron beam deposited tin doped In_2O_3 films which are accompanied with heat treatments in low-level oxygen concentration have a good potential for high conductive and transparent window applications.
5. We showed that the Mott-Schottky theory is well satisfied for nonostructured lowly tin doped In_2O_3 films semiconductor.
6. The trace amount of impurities were formed an unwanted p-type semiconductive behaviour at high frequency of EIS data, therefore the control of impurities level is very important.
7. Transmittance studies showed that the lowly tin doped In_2O_3 film is indirect semiconductor. The calculated allowed indirect optical band gap for our case was ca. 3.80 eV.
8. A comparison between the quantum efficiency of the lowly tin doped In_2O_3 and polycrystalline GaP showed that the reduction in grain size increased the optical band gap which in turn will cause a decrease in electron-hole recombination and finally an increasing in the quantum efficiency of nonostructured films.

References

1. S. Sapra, J. Nanda, D. D. Sarma, *Semiconducting Nanoparticles*, Solid State and Structural Chemistry Unit, Indian Institute of Science, Bangalore – 560 012, India.
2. A. P. Alivisatos, *J. Phys. Chem.***1996**, 100, 13226–13239.
3. S. K. Poznyak, A. I. Kulak, *Electrochim. Acta* **2000**, *45*, 1595–1605.
4. S. K. Poznyak, A. N. Golubev, A. I. Kulak, *Surface Science* **2000**, 454–456, 396–401.
5. M. Metikos-Hukovic, S. Omanovic, *J. Electroanal. Chem.* **1998**, *455*, 181–189.
6. J. H. Kennedy, K. W. Frese, *J. Electrochem. Soc.* **1978**, *125*, 723–726.
7. Y. Meng, X. Yang, H. Chen, J. Shen, Z. Zhang, Z. Hua, *Thin Solid Film* **2001**, *394*, 219–223.
8. E. Bertran, C. C. Corbella, M. Vives, A. Pinyol, C. Person, I. Porqueras, *Solid State Ionic* **2003**, *165*, 139–148.
9. B. J. Chen, X. W. Sun, B. K. Tay, *Materials Science and Engineering B* **2004**, *106*, 300–304.
10. H. K. Jang, S.W. Whangbo, Y.K. Choi, K. Jeong, C. N. Whang, C.H. Wang, D. J. Choi, S. Lee, *Journal of Non-Crystalline Solids* **2001**, *296*, 182–187.
11. M. Girtan, G. I. Rusu, G. G. Rusu, S. Gurlui, *Applied Surface Scince* **2000**, *162–163*, 492–498.
12. T. Tsuchiya, H. Niino, A. Yabe, I. Yamaguchi, T. Manabe, T. Kumagi, S. Mizuta, *Applied Surface Scince* **2002**, *197–198*, 512–515.
13. A. L. Dawar, J. C. Joshi, *J. Mater. Sci*. **1984**, *19*, 1–23.
14. Zview: Impedance/Gain phase Graphics and Analysis Software, Scribner Associates, Charlottesville, VA, 1993.
15. M. Metikos-Hukovic, S. Omanovic, A. Jukic, *Electrochim. Acta* **1999**, *45*, 977–986.

16. S. M. Sze, *Physics of semiconductor devices*, John Wiley & Sons, Inc., 2nd edition, 1981, pages 516 and 517.
17. J. P. McKelvey, *Solid state and semiconductor physics*, Harper & Row, New York, 1966, page 472.
18. D. D. Macdonald, E. Sikora, G. Engelhardt, *Electrochim. Acta* **1998**, *43*, 87–107.
19. J. Sikora, E. Sikora, D. D. Macdonald, *Electrochim. Acta* **2000**, *45*, 1875–1883.
20. Princeton applied research, Application note AC-1"Basic of electrochemical impedance spectroscopy (EIS)" pp 8–9.
21. W. P. Gomes, D. Vanmaekelbergh, *Electrochimica Acta* **1996**, *41*, 967–973.
22. T. Gerfin, M. Gratzel, *J. Sppl. Phys.* **1996**, *79*, 1722–1729.
23. D. F. Shriver, P. W. Atkins, C. H. Langford, Freeman, 1990, page 101.
24. H. Morikawa, M. Fujita, *Thin Solid Film* **2000**, *359*, 61–67.
25. A. L. Dawar, J. C. Joshi, *J. Mater. Sci*. **1984**, *19*, 1–23.
26. J. J. Kelly, D. Vanmaekelbergh, *Electrochim. Acta* **1998**, *43*, 2773–2780.
27. W. W. Gärtner, *Phys. Rev.* **1959**, *116*, 84–87.

Appendix. List of used symbols with corresponding units.

Physical Properties	Symbol	Unit
Grain size	D	nm
Reflection angle	θ	degree
Wavelength	λ	Å
Full width at half maximum	FWHM or B	degree or radian
Peak voltage	E_p	Volt
Peak current	I_p	Amp.
Valley voltage	E_v	volt
Valley current	I_v	Amp.
Imaginary component of impedance	Z”	ohm
Real component of impedance	Z’	ohm
Constant phase element impedan	Z_{CPE}	ohm

Physical Properties	Symbol	Unit
Warburg diffusion coefficient	σ	ohm $(\text{rad s}^{-1})^{1/5}$
Effective diffusion length	L	m
Diffusion coefficient	D	$\text{Cm}^2\ \text{s}^{-1}$
Flat band potential	E_{FB}	Volt
Donor concentration	N_D	cm^{-3}
Acceptor concentration	N_A	cm^{-3}
Space charge layer capacitance	C_{sc}	F cm^{-2}
Space charge layer width	W_{sc}	nm
Absorption coefficient	α(λ)	nm^{-1}
Quantum efficiency	Q	----------

Povzetek

Elektronske lastnosti nanostrukturnih plasti In_2O_3, dopiranih s kositrom (ITO), ki smo jih pripravili z metodo naparevanja z elektronskim curkom, smo raziskovali s polarizacijskim krivuljami in elektrokemijsko impedančno spektroskopijo v 0,5 mol dm^{-3} H_2SO_4. Rezultati diferencialne kapacitivnosti kažejo, da v visoko frekvenčnem območju ITO ali dopirni elementi lahko razvijejo p-n vez (Esaki tunelska dioda) z nizko koncentracijo nosilcev naboja, i.e., $N_D = 2.07\times10^9$ cm^{-3} in $N_A = 1.38\times10^9$ cm^{-3}. V nizko frekvenčnem območju prihaja do tvorbe samo n-tipa polprevodnika. Potencial ravnega pasu E_b, ki smo ga določili iz meritev kapacitivnosti, je v nizko frekvenčnem območju okrog –0,034 V proti NKE. Iz naklona lineranega dela Mott-Schottky krivulje smo izračunali koncentracijo nosilcev naboja $N_D = 7.1501\times10^{21}$ cm^{-3}.